Supplementary information

Self-Supporting Composited Electrocatalysts of Ultrafine Mo_2C on 3D-Hierarchical Porous Carbon Monoliths for Efficient Hydrogen Evolution

Haiyang Lu[a], Boxu Gao[a], Hongbin Zhang[b*], Xueliang Fan[a], Luyao Zheng[a], Jingwen Tan[c], Sinong Wang[b], Yahong Zhang[a], Qingsheng Gao[c*], Yi Tang[a*]

a. Department of Chemistry, Shanghai Key Laboratory of Molecular Catalysis and Innovative Materials, Laboratory of Advanced Materials and Collaborative Innovation Center of Chemistry for Energy Materials, Fudan University, Shanghai 200433, China. E-mail: yitang@fudan.edu.cn
b. Institute for Preservation of Chinese Ancient Books, Fudan University Library, Fudan University, Shanghai 200433, China. E-mail: zhanghongbin@fudan.edu.cn
c. Department of Chemistry, Jinan University, Guangzhou 510632, China. E-mail: tqsgao@jnu.edu.cn

Calculation of Mo_2C content

A combustion reaction during the heating process can eliminate all the carbon elements and transform Mo_2C into MoO_3.[1] Thus, the content of Mo elements and Mo_2C can be further calculated through MoO_3 content according to the following equation:

$$m_{Mo_2C}\% = \frac{m_{residual}\% \times M(Mo_2C)}{2 \times M(MoO_3)}$$

Take 3D Mo_2C/PCM-4 for example, $m_{Mo_2C}\% = \frac{49\% \times 204}{2 \times 144} = 34.7\%$. The atomic percentage of Mo is calculated to be 5.7 at.%.

Calculation of the surface fraction of Mo_2C

From the integrated area of the anodic wave as shown in Fig. 5e, we derive a charge of Q = 15.896 C passed during the irreversible oxidation of Mo_2C to MoO_3 following a 16-electron process:[1–3]

$$Mo_2C + 9H_2O \rightarrow 2MoO_3 + CO_3^{2-} + 18H^+ + 16e^-$$

$$n_{sruface} = \frac{Q}{nF} = \frac{15.896\ C}{16 \times 96500} = 1.03 \times 10^{-5}\ mol$$

$$n_{total} = \frac{mw}{M_w} = \frac{0.00928\ g \times 34.7\%}{203.88\ g/mol} = 1.58 \times 10^{-5}\ mol$$

$$f = \frac{n_{sruface}}{n_{total}} = \frac{1.03 \times 10^{-5}}{1.58 \times 10^{-5}} = 65.2\%$$

Where n = 16 is the number of electron transferred, F is the Faraday constant, m is the mass of the self-supporting 3D Mo_2C/PCM-4 electrode, w is the weight fraction of Mo_2C obtained from TGA, M_w is the molecular weight of Mo_2C, and f is the exposed surface fraction of Mo_2C in 3D Mo_2C/PCM-4.

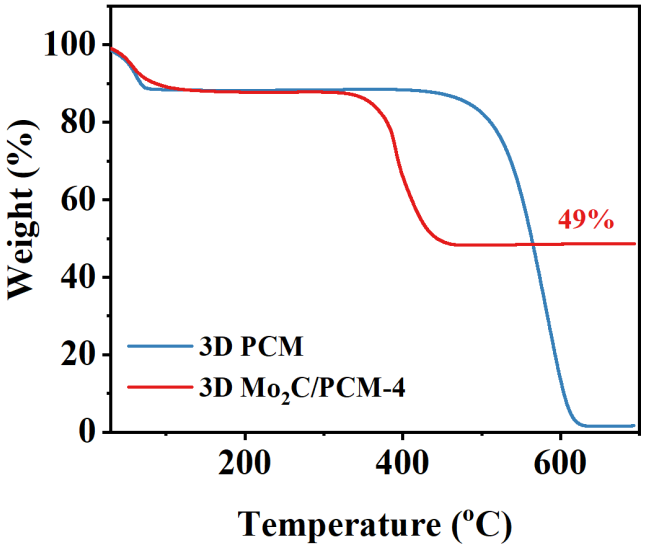

Fig. S1 TGA plots of 3D PCM and 3D Mo_2C/PCM-4 under the air atmosphere.

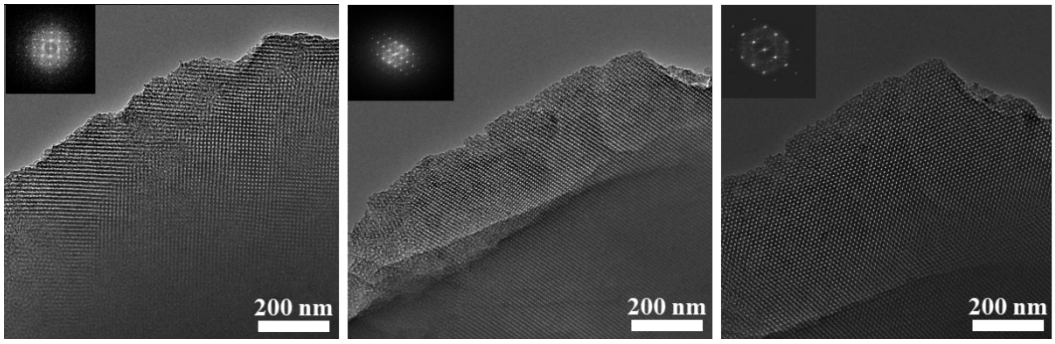

Fig. S2 TEM images of 3D PCM, viewed from [100], [110], and [111] directions and its corresponding fast Fourier transform (FFT) diffractograms.

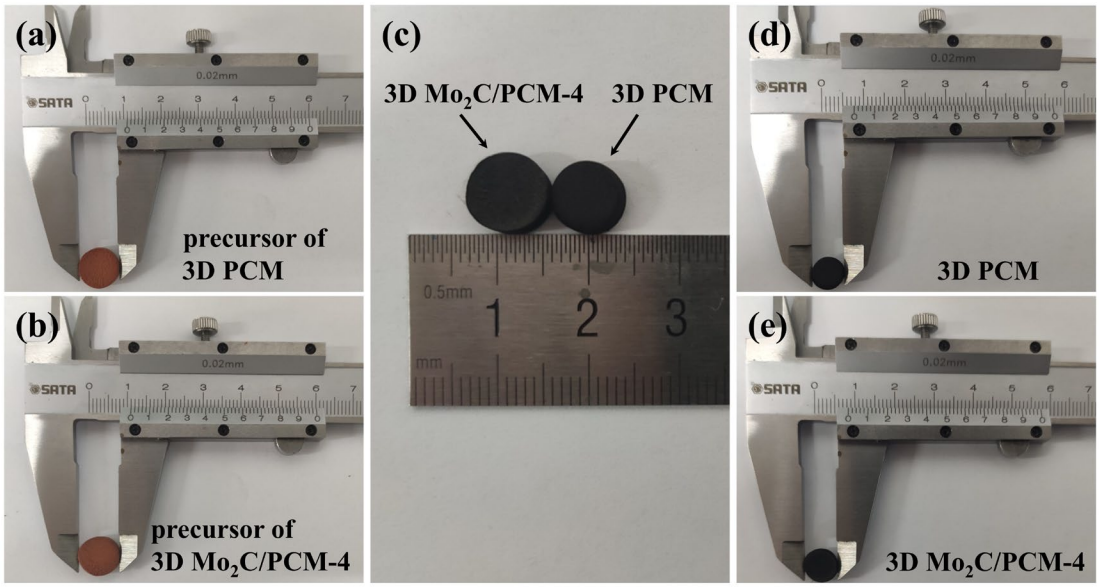

Fig. S3 Optical photos of materials: (a) precursor of 3D PCM, (b) precursor of 3D Mo_2C/PCM-4, (c) comparison of 3D PCM and 3D Mo_2C/PCM-4, (d) 3D PCM, and (e) 3D Mo_2C/PCM-4.

As shown in Fig. S3a-b, the diameter of the two disc-shaped precursors are 11.00 mm. And after annealing treatment at 800 °C, the volume of the two shrinks to different degrees evidently (Fig. S3c). Specifically, the diameter of 3D PCM is 7.86 mm (Fig. S3d), while the diameter of 3D Mo_2C/PCM-4 is 8.44 mm (Fig. S3e). Thus, we believe that the rigid inorganic Mo species hindering the shrinkage of the precursor during the annealing treatment, resulting in a little peak shift in SAXS between 3D PCM and 3D Mo_2C/PCM-4.

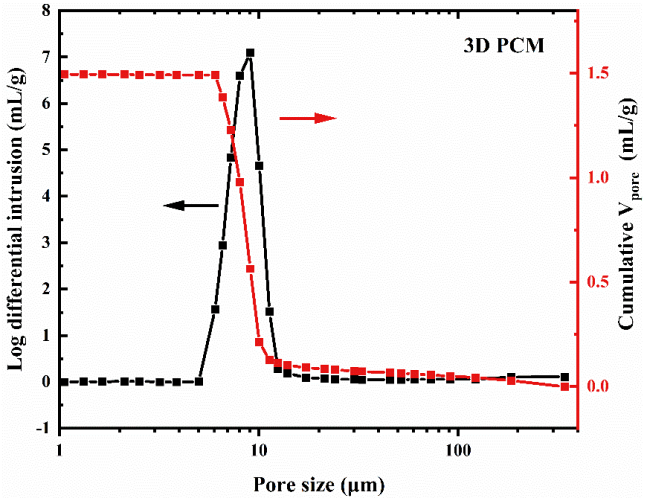

Fig. S4 Hg intrusion curve and differential PSD of 3D PCM.

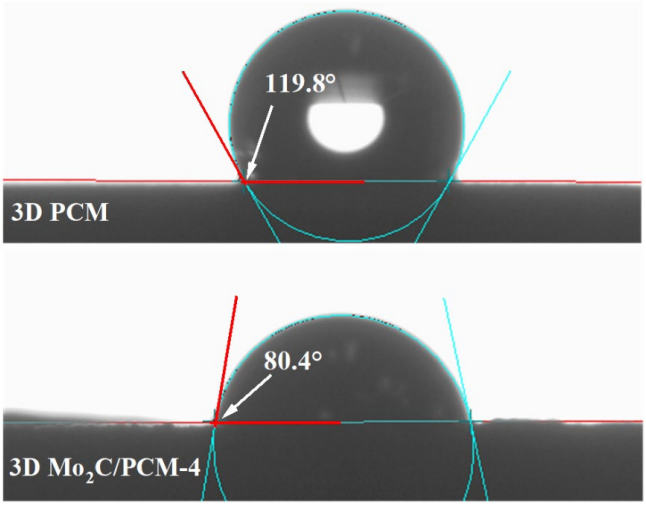

Fig. S5 Water contact angle measurements of 3D PCM powder and 3D Mo_2C/PCM-4 powder.

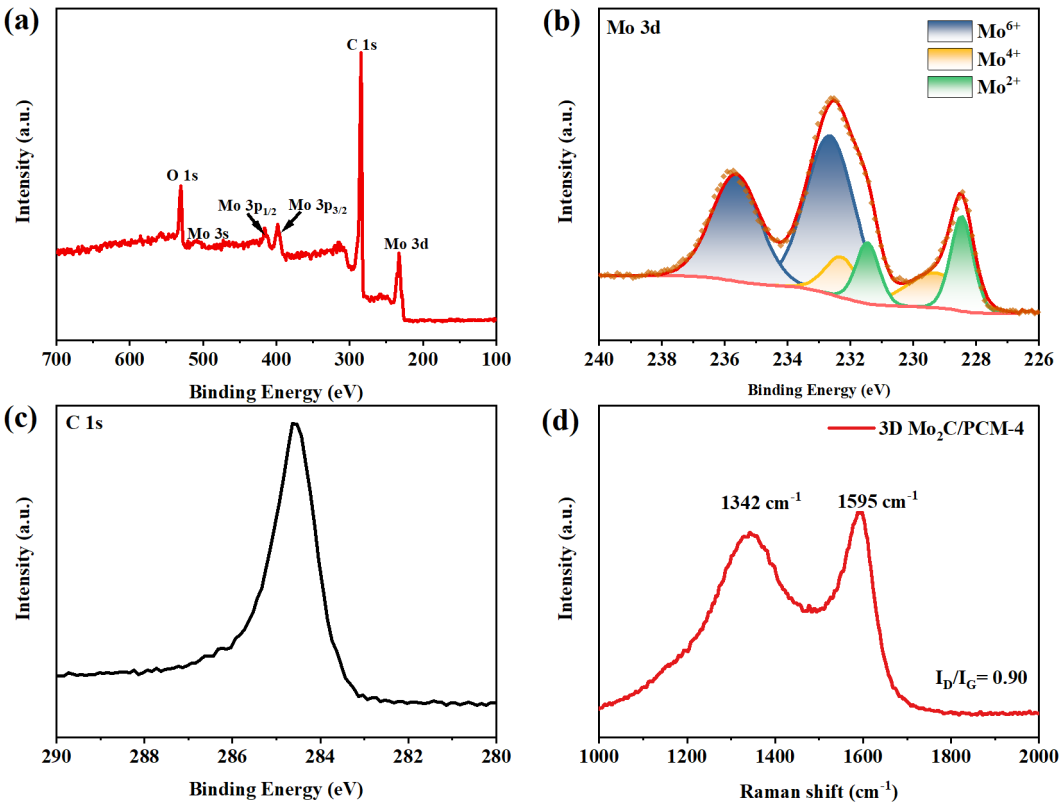

Fig. S6 (a) XPS Survey spectrum of 3D Mo_2C/PCM-4. (b) Fine spectrum of Mo 3d, and (c) high-resolution spectrum of C 1s. (d) Raman spectrum of 3D Mo_2C/PCM-4.

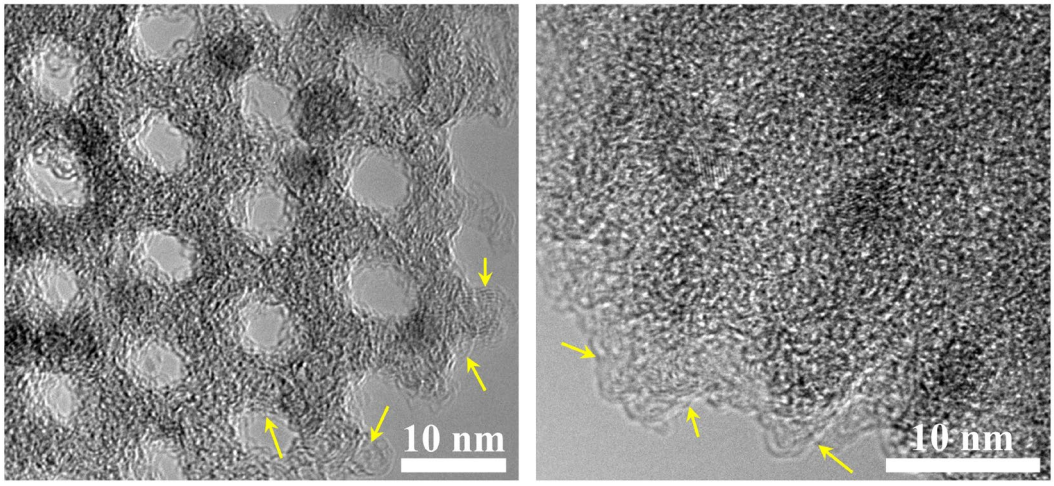

Fig. S7 TEM images of 3D Mo_2C/PCM-4.

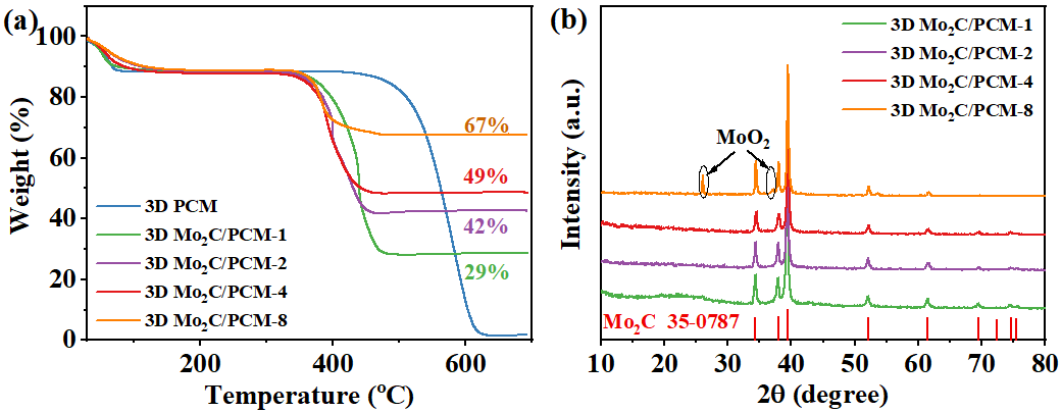

Fig. S8 (a) TGA plots of 3D PCM and 3D Mo_2C/PCMs under the air atmosphere. (b) XRD patterns of 3D Mo_2C/PCMs.

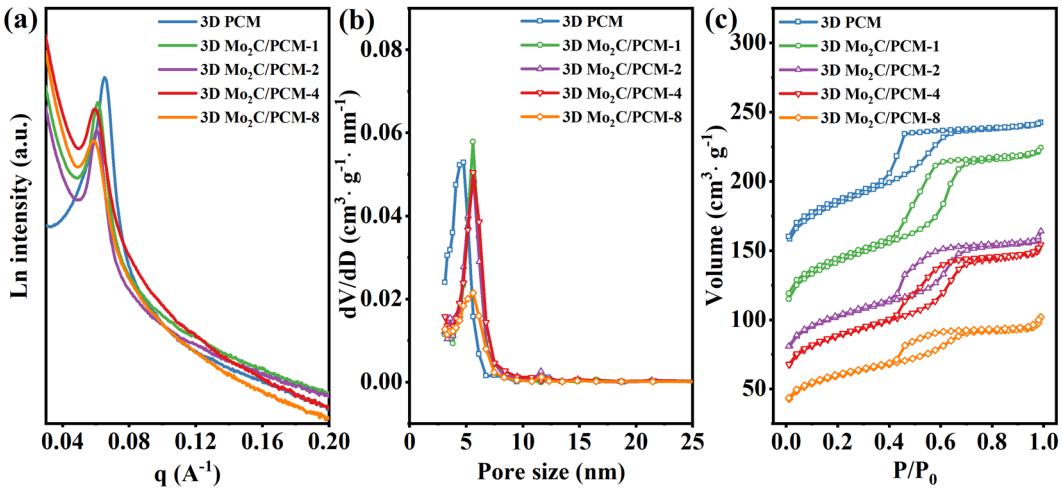

Fig. S9 (a) SAXS patterns, (b) pore size distribution curves, and (c) N_2 sorption isotherms of 3D PCM and 3D Mo_2C/PCMs.

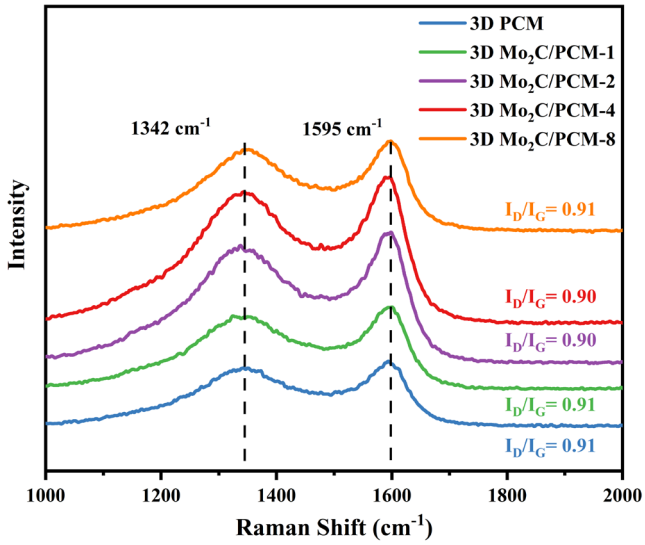

Fig. S10 Raman spectra of 3D PCM and 3D Mo_2C/PCMs.

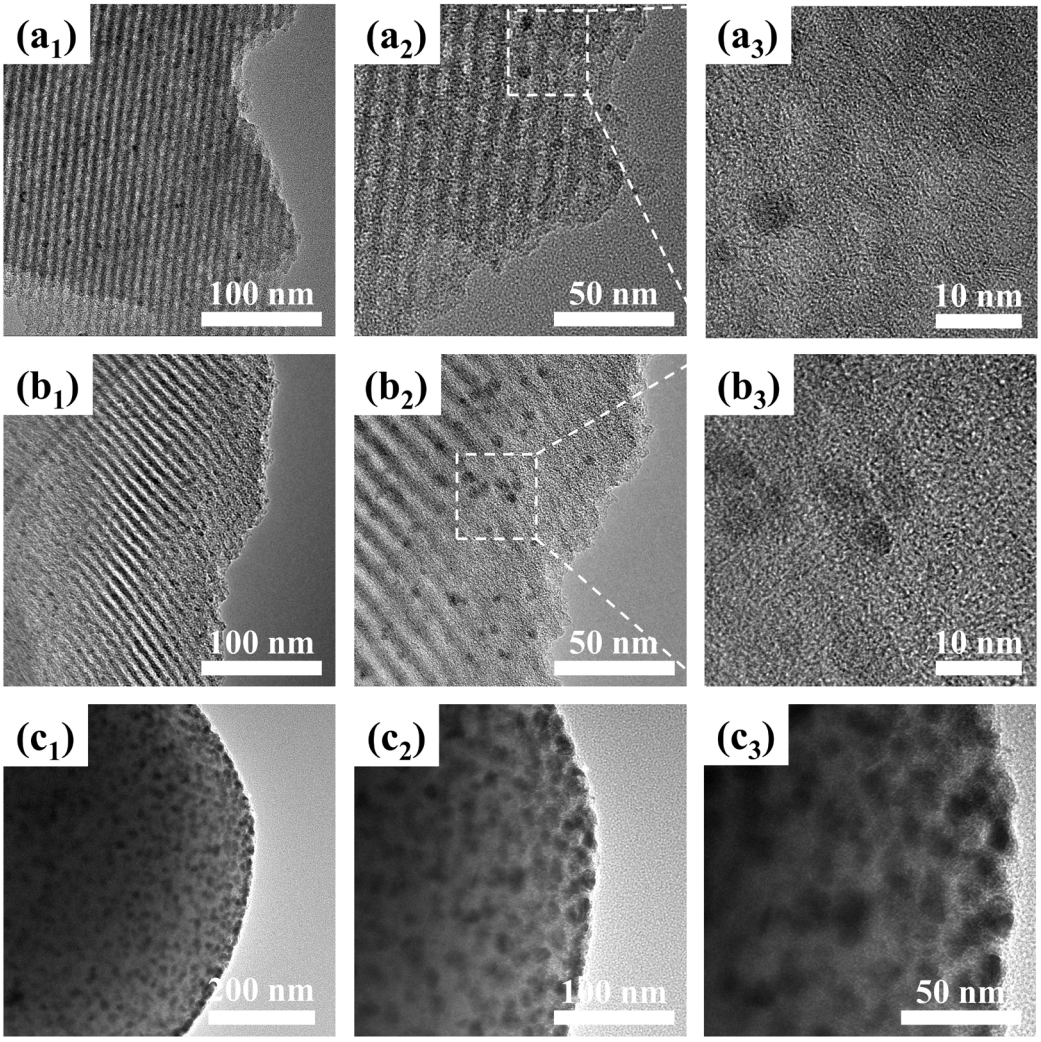

Fig. S11 (a_1 - a_3) TEM images of 3D Mo_2C/PCM-1, (b_1 - b_3) TEM images of 3D Mo_2C/PCM-2, and (c_1 - c_3) TEM images of 3D Mo_2C/PCM-8.

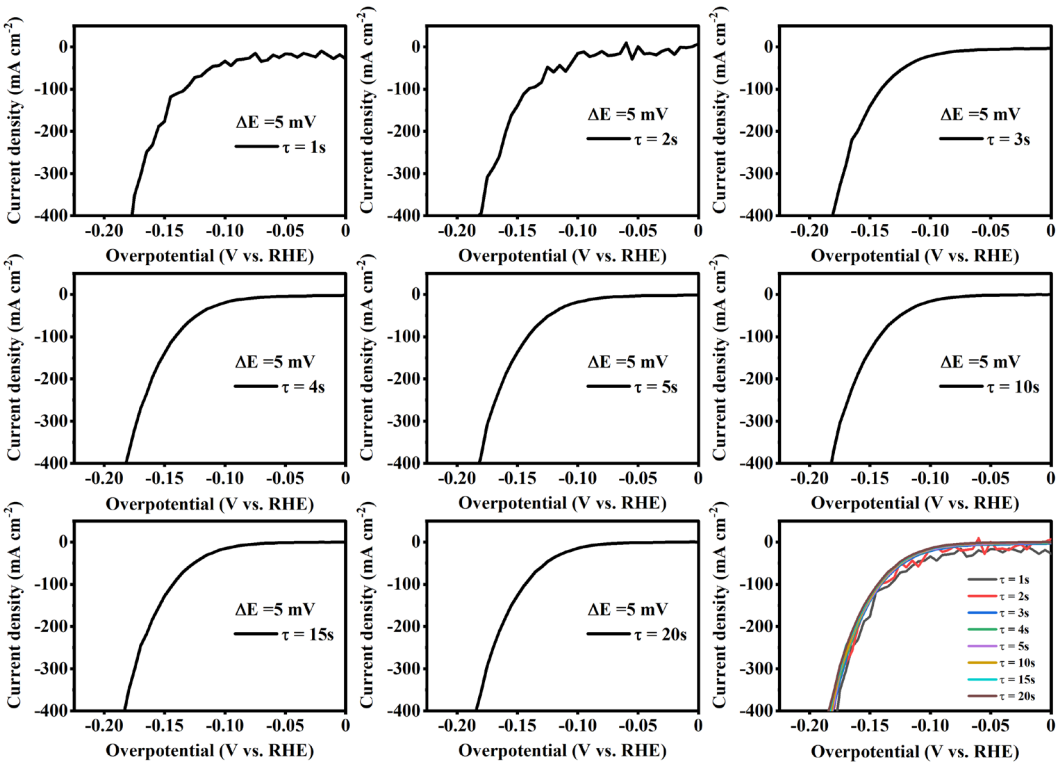

Fig. S12 Polarization curves of 3D Mo_2C/PCM-4 recorded by staircase voltammetry (SCV) at a step height (ΔE) of 5 mV with different step period (τ) in 0.5 M H_2SO_4.

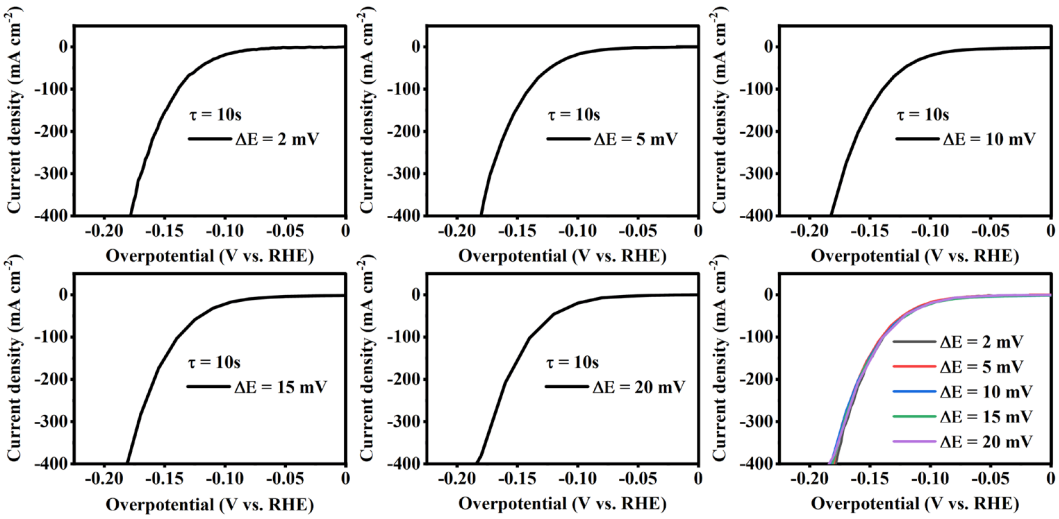

Fig. S13 Polarization curves of 3D Mo_2C/PCM-4 recorded by staircase voltammetry (SCV) at a step period (τ) of 10s with different step height (ΔE) in 0.5 M H_2SO_4.

Explanation of Fig. S12 and Fig. S13. Multiple SCV curves under different ΔE and different step periods to check the parameters of SCV method. Here, taking 3D Mo_2C/PCM-4 as the model sample, the curves were measured by SCV at a step height (ΔE) of 5 mV with different step period (τ), as shown in Fig. S12. When the step periods (τ) is too short (τ = 1, 2 s), the charging current caused by electrical double layers cannot be effectively eliminated, thus the polarization curves are not smooth and stable. When the τ exceeds 4 s, the curves can be well stabilized, and there is no obvious

difference of curves among different τ. What's more, Fig. S13 displays the curves of at a fixed τ of 10 s with different ΔE. It is clear that in the ΔE range of 2 to 20 mV, a step period of 10 s is sufficient to stabilize the polarization curve. In summary, the experimental parameters we adopted in SCV method (a ΔE of 5 mV and a step period of 10 s) is reasonable and can help us to obtain genuine HER activity.

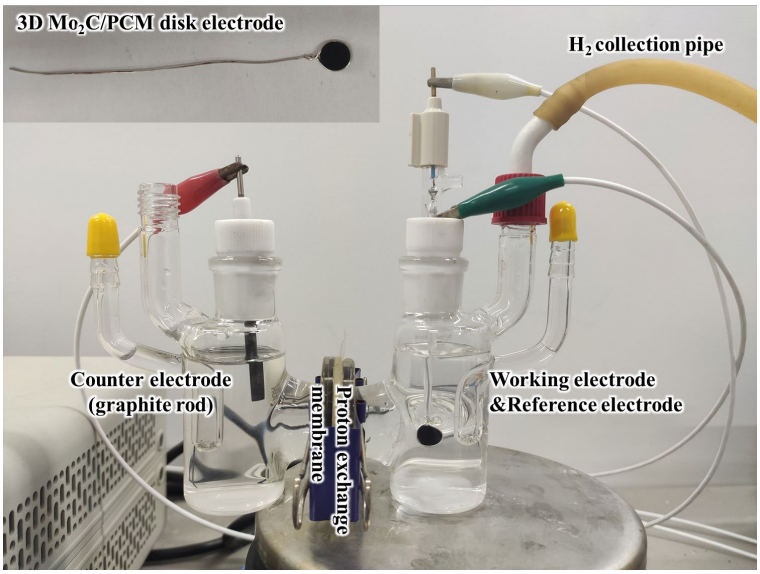

Fig. S14 Optical photo of reaction device with proton exchange membrane (inset: the as-made 3D Mo_2C/PCM disk electrode).

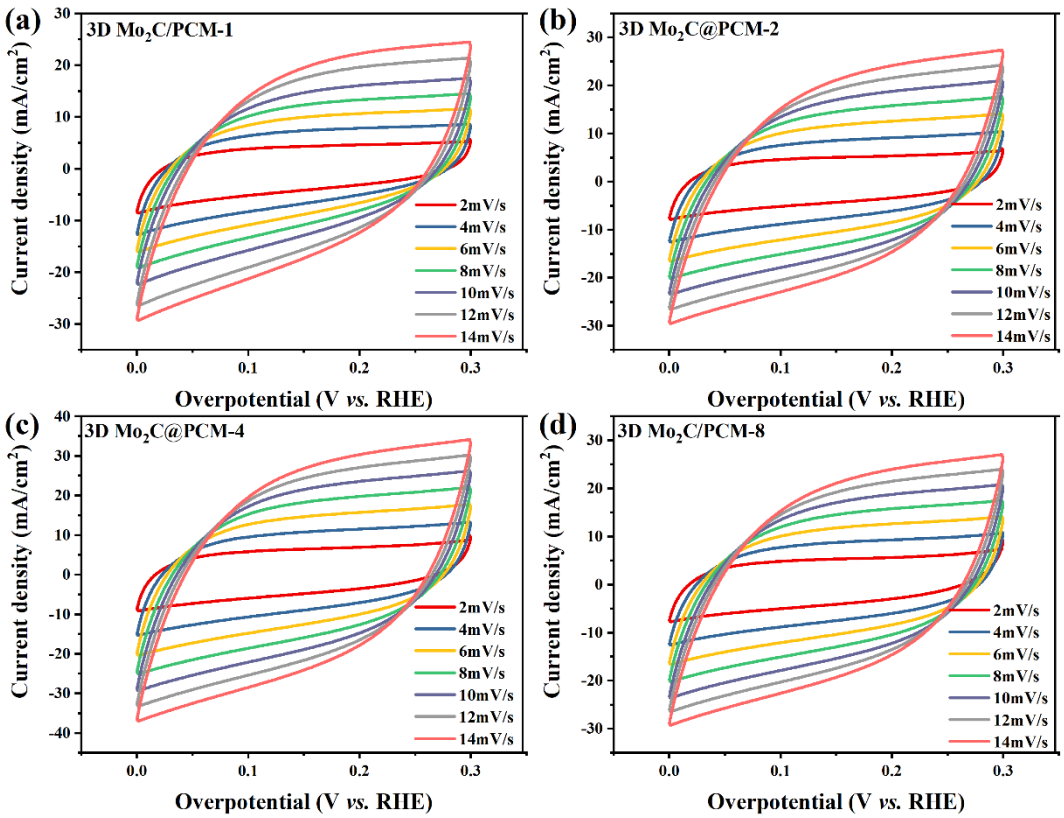

Fig. S15 CV curves of 3D Mo_2C/PCMs at different scan rates (2, 4, 6, 8, 10, 12, and 14 mV/s).

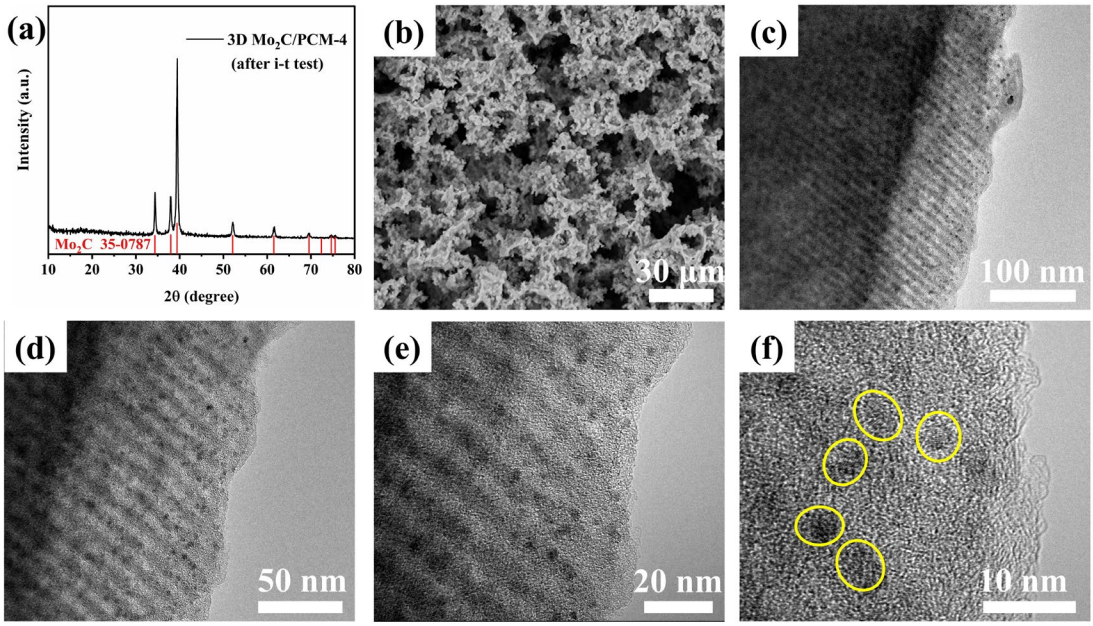

Fig. S16 (a) XRD pattern, (b) SEM image, and (c - f) TEM images of 3D Mo_2C/PCM-4 after the stability test.

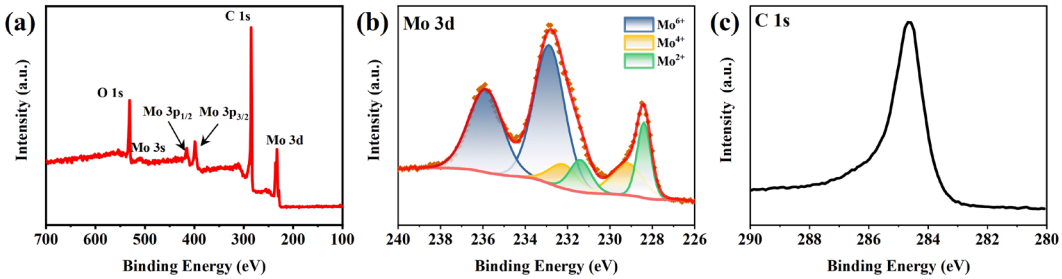

Fig. S17 The XPS spectra of 3D Mo_2C/PCM-4 after long-time stability test: (a) XPS survey, (b) fine spectrum of Mo 3d and (c) high-resolution spectrum of C 1s.

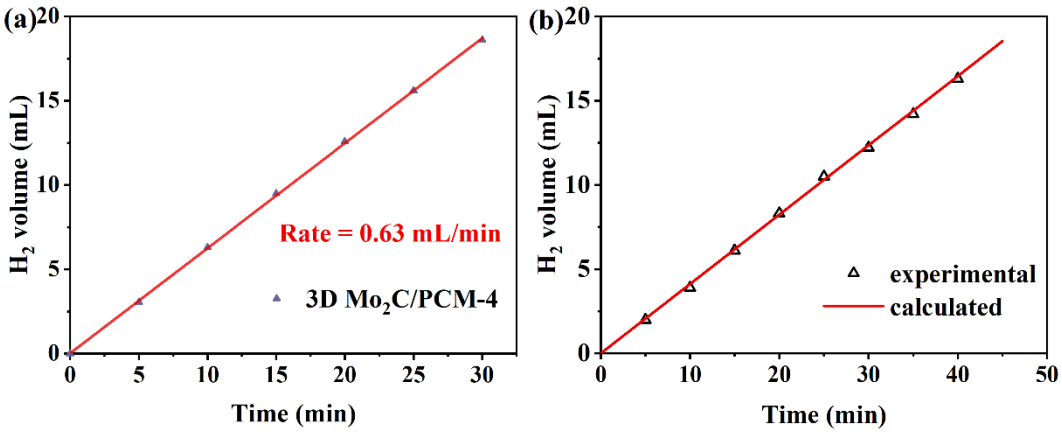

Fig. S18 (a) The plot of measured H_2 volume versus time for 3D Mo_2C/PCM-4 at 300 mV. (b) Faradic efficiency test of 3D Mo_2C/PCM-4 by plotting experimental H_2 volume and theoretical H_2 volume against time at the current of 60 mA.

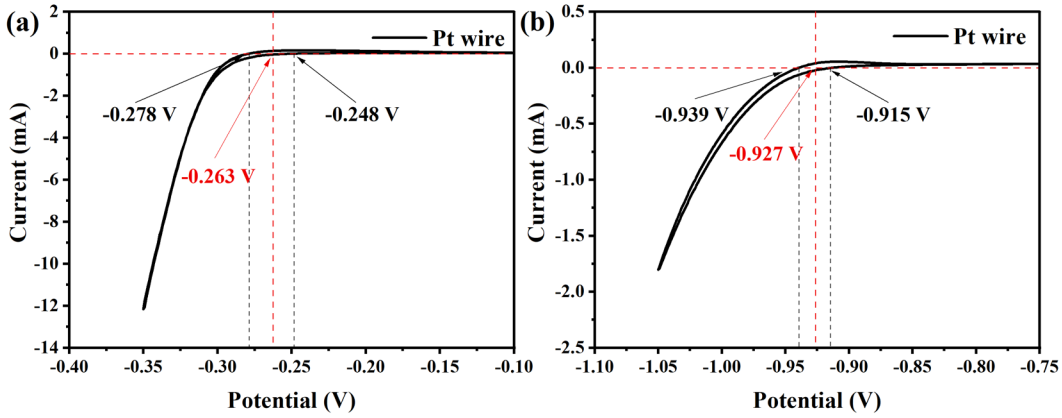

Fig. S19 Calibration of (a) a saturated calomel electrode (SCE) and (b) a mercury oxide electrode (Hg/HgO) potential using a reversible hydrogen electrode (RHE) by CV curve at scan rate of 2 mV/s in 0.5 M H_2SO_4 and 1.0 M KOH, respectively.

The potential of reference electrode was calibrated with respect to a reversible hydrogen electrode (RHE), which was performed in a high-purity H_2 (99.999%) saturated electrolyte with a Pt wire as the working electrode and counter electrode. And then cyclic voltammograms (CVs) were collected at a scan rate of 2 mV s^{-1}, and the average of the two potentials at which the current crossed zero was taken as the thermodynamic potential for the hydrogen electrode reactions. As shown in Fig. S19, in 0.5 M H_2SO_4, E(RHE) = E(SCE) + 0.263, and in 1.0 M KOH, E(RHE) = E (Hg/HgO) – 0.927, which were consistent with the result calculated by Nernst equation.

Table S1 Textual parameters of 3D PCM and 3D Mo_2C/PCMs

Catalysts	S_{BET} (m^2/g)	D_{meso} (nm)	V_{total} (cm^3/g)	V_{mic} (cm^3/g)	Mo_2C content (wt. %)
3D PCM	695	4.8	0.375	0.175	0
3D Mo_2C/PCM-1	532	5.6	0.347	0.146	20.5
3D Mo_2C/PCM-2	378	5.6	0.254	0.106	29.7
3D Mo_2C/PCM-4	321	5.6	0.234	0.089	34.7
3D Mo_2C/PCM-8	215	5.6	0.158	0.051	47.5

Table S2 Summary of the HER activity of 3D Mo_2C/PCMs in 0.5 M H_2SO_4.

Catalysts	η_{10} (mV)	η_{100} (mV)	Tafel slope (mV/decade)	j_0 (mA/cm^2)	C_{dl} (mF/cm^2)	R_{ct} (Ω)
3D Mo_2C/PCM-1	124	214	102	0.34	1177	14.8
3D Mo_2C/PCM-2	100	193	90	0.40	1285	6.2
3D Mo_2C/PCM-4	81	146	63	0.51	1649	1.7
3D Mo_2C/PCM-8	93	163	72	0.37	1302	2.6

Table S3. Comparison of HER performance for 3D Mo_2C/PCM with other electrocatalysts in acidic electrolytes.

Catalysts	Electrolytes	*j* (mA/cm^2)	η (mV)	Tafel slope (mV/dec)	Ref.
3D Mo_2C/PCM	0.5 M H_2SO_4	10	81	63	This work
Mo_2C/CC	0.5 M H_2SO_4	10	140	124	4
Mo_2C-MoOx/CC	1.0 M $HClO_4$	10	60	53	5
Mo_2C nanoribbon/N-G	0.5 M H_2SO_4	10	162	57	6
Mo_2C@CC	0.5 M H_2SO_4	10	106	54	7
Mo_2C/G	0.5 M H_2SO_4	10	166	80	8
3DHP-Mo_2C	0.5 M H_2SO_4	10	166	75	9
np-η-MoC NSs	0.5 M H_2SO_4	10	122	53	10
vMo_xC-Ar-O150-*c*	0.5 M H_2SO_4	10	130	-	11
Mo_2C@N-CANs	0.5 M H_2SO_4	10	82	66	12
Mo_2C/G	0.5 M H_2SO_4	10	175	88	8
Mo_2C@OCM	0.5 M H_2SO_4	10	160	51	1
Mo_2C/G3-NCS	0.5 M H_2SO_4	10	70	39	13
Mo_2C-graphene	0.5 M H_2SO_4	10	150	57	14
Mo_2C/NCF	0.5 M H_2SO_4	10	144	55	2
Mo_2C@N-CNFs	0.5 M H_2SO_4	10	167	70	15
Mo_2C/GNRs	0.5 M H_2SO_4	10	152	65	16
Mo_2C@N-doped C	0.5 M H_2SO_4	10	124	60	17
Mo_xC@3D N-doped C	0.5 M H_2SO_4	10	89	51	18
Mo_2C/N-doped CNT	0.5 M H_2SO_4	10	147	71	19
Mo_2C microparticles	0.5 M H_2SO_4	20	ca. 225	55	20
MoC@graphite shell	0.5 M H_2SO_4	10	124	43	21
MoC_x octahedrons	0.5 M H_2SO_4	10	142	53	22
Mo_2C nanowires	0.5 M H_2SO_4	10	130	53	23
Mo_2C nanotubes	0.5 M H_2SO_4	10	172	34	24
$MoCT_x$ (Mxenes)	0.5 M H_2SO_4	10	283	-	25
3D hierarchical porous Mo_2C	0.5 M H_2SO_4	10	97	60	26
Mo_xC-IOL	0.5 M H_2SO_4	10	117	60	27

Table S4. Comparison of HER performance for 3D Mo_2C/PCM with other electrocatalysts in alkaline electrolytes.

Catalysts	Electrolytes	j (mA/cm^2)	η (mV)	Tafel slope (mV/dec)	Ref.
3D Mo_2C/PCM	1.0 M KOH	10	47	45	This work
Mo_2C/CC	1.0 M KOH	10	140	124	4
Mo_2C-MoOx/CC	1.0 M KOH	10	60	53	5
Mo_xC/Cu	1.0 M KOH	10	136	98.3	28
Mo_2C nanoribbon/N-G	1.0 M KOH	10	162	57	6
Mo_2C@CC	1.0 M KOH	10	72	52	7
Mo_2C/G	1.0 M KOH	10	161	76	8
Mo_2C/N-CNFs	1.0 M KOH	10	168	47	15
np-η-MoC NSs	1.0 M KOH	10	119	39	10
Mo_2C/NCF	1.0 M KOH	10	100	65	2
Mo_2C/GNRs	1.0 M KOH	10	121	54	16
Mo_2C@N-doped C	1.0 M KOH	10	78	41	17
Mo_2C@3D N-doped C	1.0 M KOH	10	122	78	18
3DHP-Mo_2C	1.0 M KOH	10	139	71	9
vMo_xC-Ar-O150-*c*	1.0 M KOH	10	116	-	11
Mo_2C@N-CANs	1.0 M KOH	10	100	76	12
Mo_2C@MCS	1.0 M KOH	10	134	51	3
Mo_2C/G	1.0 M KOH	10	200	82	8
Mo_2C@OCM	1.0 M KOH	10	175	64	1
Mo_2C microparticles	1.0 M KOH	10	210-240	5-59	20
Mo_2C nanoparticles	1.0 M KOH	10	176	58	29
MoC@graphite shell	1.0 M KOH	10	76	50	21
MoC_x octahedrons	1.0 M KOH	10	151	59	22
Mo_2C nanotubes	0.1 M KOH	10	117	55	24
Skeletal Mo_xC	1.0 M KOH	10	101	44	30
Mo_xC-IOL	0.1 M KOH	10	82	56	27

† The yellow area represents self-supporting Mo_xC, the green area represents Mo_xC-carbon, and the light blue area represents nanosized Mo_xC.

References

1 J. Wang, W. Wang, L. Ji, S. Czioska, L. Guo and Z. Chen, *ACS Appl. Energy Mater.*, 2018, **1**, 736–743.

2 Y. Huang, Q. Gong, X. Song, K. Feng, K. Nie, F. Zhao, Y. Wang, M. Zeng, J. Zhong and Y. Li, *ACS Nano*, 2016, **10**, 11337–11343.

3 S. Yuan, S. Xu, Z. Liu, G. Huang, C. Zhang, J. Ai, X. Li and N. Li, *ChemCatChem*, 2019, **11**, 2643–2648.

4 M. Fan, H. Chen, Y. Wu, L.-L. Feng, Y. Liu, G.-D. Li and X. Zou, *J. Mater. Chem. A*, 2015, **3**, 16320–16326.

5 L. He, W. Zhang, Q. Mo, W. Huang, L. Yang and Q. Gao, *Angew. Chemie Int. Ed.*, 2020, **59**, 3544–3548.

6 J. Gao, Z. Cheng, C. Shao, Y. Zhao, Z. Zhang and L. Qu, *J. Mater. Chem. A*, 2017, **5**, 12027–12033.

7 M. He, H. Shi, P. Wang, X. Sun and B. Gao, *Chem. – A Eur. J.*, 2019, **25**, 16106–16113.

8 H. Huang, C. Yu, H. Huang, W. Guo, M. Zhang, X. Han, Q. Wei, S. Cui, X. Tan and J. Qiu, *Small Methods*, 2019, **3**, 1900259.

9 T. Meng, L. Zheng, J. Qin, D. Zhao and M. Cao, *J. Mater. Chem. A*, 2017, **5**, 20228–20238.

10 C. Tang, H. Zhang, K. Xu, Q. Zhang, J. Liu, C. He, L. Fan and T. Asefa, *J. Mater. Chem. A*, 2019, **7**, 18030–18038.

11 S. Kim, C. Choi, J. Hwang, J. Park, J. Jeong, H. Jun, S. Lee, S.-K. Kim, J. H. Jang, Y. Jung and J. Lee, *ACS Nano*, 2020, **14**, 4988–4999.

12 Q. Kang, M. Li, Z. Wang, Q. Lu and F. Gao, *Nanoscale*, 2020, **12**, 5159–5169.

13 H. Wei, Q. Xi, X. Chen, D. Guo, F. Ding, Z. Yang, S. Wang, J. Li and S. Huang, *Adv. Sci.*, 2018, **5**, 1700733.

14 C. He and J. Tao, *Chem. Commun.*, 2015, **51**, 8323–8325.

15 Z.-Y. Wu, B.-C. Hu, P. Wu, H.-W. Liang, Z.-L. Yu, Y. Lin, Y.-R. Zheng, Z. Li and S.-H. Yu, *NPG Asia Mater.*, 2016, **8**, e288–e288.

16 X. Fan, Y. Liu, Z. Peng, Z. Zhang, H. Zhou, X. Zhang, B. I. Yakobson, W. A. Goddard, X. Guo, R. H. Hauge and J. M. Tour, *ACS Nano*, 2017, **11**, 384–394.

17 Y. Liu, G. Yu, G.-D. Li, Y. Sun, T. Asefa, W. Chen and X. Zou, *Angew. Chemie Int. Ed.*, 2015, **54**, 10752–10757.

18 H. Zhang, Z. Ma, G. Liu, L. Shi, J. Tang, H. Pang, K. Wu, T. Takei, J. Zhang, Y. Yamauchi and J. Ye, *NPG Asia Mater.*, 2016, **8**, e293–e293.

19 K. Zhang, Y. Zhao, D. Fu and Y. Chen, *J. Mater. Chem. A*, 2015, **3**, 5783–5788.

20 H. Vrubel and X. Hu, *Angew. Chemie Int. Ed.*, 2012, **51**, 12703–12706.

21 Z. Shi, Y. Wang, H. Lin, H. Zhang, M. Shen, S. Xie, Y. Zhang, Q. Gao and Y. Tang, *J. Mater. Chem. A*, 2016, **4**, 6006–6013.

22 H. Bin Wu, B. Y. Xia, L. Yu, X.-Y. Yu and X. W. (David) Lou, *Nat. Commun.*, 2015, **6**, 6512.

23 L. Liao, S. Wang, J. Xiao, X. Bian, Y. Zhang, M. D. Scanlon, X. Hu, Y. Tang, B. Liu and H. H. Girault, *Energy Environ. Sci.*, 2014, **7**, 387–392.

24 F.-X. Ma, H. Bin Wu, B. Y. Xia, C.-Y. Xu and X. W. (David) Lou, *Angew. Chemie Int. Ed.*, 2015, **54**, 15395–15399.

25 Z. W. Seh, K. D. Fredrickson, B. Anasori, J. Kibsgaard, A. L. Strickler, M. R. Lukatskaya, Y. Gogotsi, T. F. Jaramillo and A. Vojvodic, *ACS Energy Lett.*, 2016, **1**, 589–594.

26 H. Ang, H. Wang, B. Li, Y. Zong, X. Wang and Q. Yan, *Small*, 2016, **12**, 2859–2865.
27 F. Li, X. Zhao, J. Mahmood, M. S. Okyay, S.-M. Jung, I. Ahmad, S.-J. Kim, G.-F. Han, N. Park and J.-B. Baek, *ACS Nano*, 2017, **11**, 7527–7533.
28 Z. Wei, X. Hu, S. Ning, X. Kang and S. Chen, *ACS Sustain. Chem. Eng.*, 2019, **7**, 8458–8465.
29 L. Ma, L. R. L. Ting, V. Molinari, C. Giordano and B. S. Yeo, *J. Mater. Chem. A*, 2015, **3**, 8361–8368.
30 Y. Wang, Z. Shi, Q. Mo, B. Gao, B. Liu, L. Wang, Y. Zhang, Q. Gao and Y. Tang, *ChemElectroChem*, 2017, **4**, 2169–2177.